



1 **A multi-centennial record of past floods and earthquakes in** 2 **Valle d'Aosta, Mediterranean Italian Alps**

3
4 Bruno Wilhelm¹, Hendrik Vogel², Flavio S. Anselmetti²

5
6 ¹University Grenoble Alpes, CNRS, IRD, Institut des Géosciences et de l'Environnement, F-38000 Grenoble,
7 France

8 ²Institute of Geological Sciences and Oeschger Centre for Climate Change Research, University of Bern, CH-
9 3012 Bern, Switzerland

10 *Correspondence to: B. Wilhelm (bruno.wilhelm@univ-grenoble-alpes.fr)*

11 **Abstract**

12 Mediterranean Alpine populations are particularly exposed to natural hazards like floods and earthquakes
13 because of both the close Mediterranean humidity source and the seismically active Alpine region. Knowledge
14 of long-term variability in flood and earthquake occurrences is of high value since it can be useful to improve
15 risk assessment and mitigation. In this context, we explore the potential of a lake-sediment sequence from Lago
16 Inferiore de Laures in Valle d'Aosta (Northern Italy) as a long-term record of past floods and earthquakes. The
17 high-resolution sedimentological study revealed 77 event layers over the last ca. 270 years; 8 are interpreted as
18 most probably induced by earthquakes and 68 by flood events. Comparison to historical seismic data suggests
19 that the recorded earthquakes are strong (epicentral MSK intensity of VI-IX) and/or close to the lake (distance of
20 25-120 km). Compared to other lake-sediment sequences, Lago Inferiore de Laures sediments appear to be
21 regionally the most sensitive to earthquake shaking, offering a great potential to reconstruct the past regional
22 seismicity further back in time. Comparison to historical and palaeoflood records suggests that the flood signal
23 reconstructed from Lago Inferiore de Laures sediments well represents the regional and (multi-)decennial
24 variability of summer-autumn floods, in connection to Mediterranean mesoscale precipitation events. Overall,
25 our results reveal the high potential of Lago Inferiore de Laures sediments to extend the regional earthquake and
26 flood catalogues far back in time.

27

28 **Key-words:** sediment record, earthquake, flood, century, Mediterranean Alps

29

30 **1. Introduction**

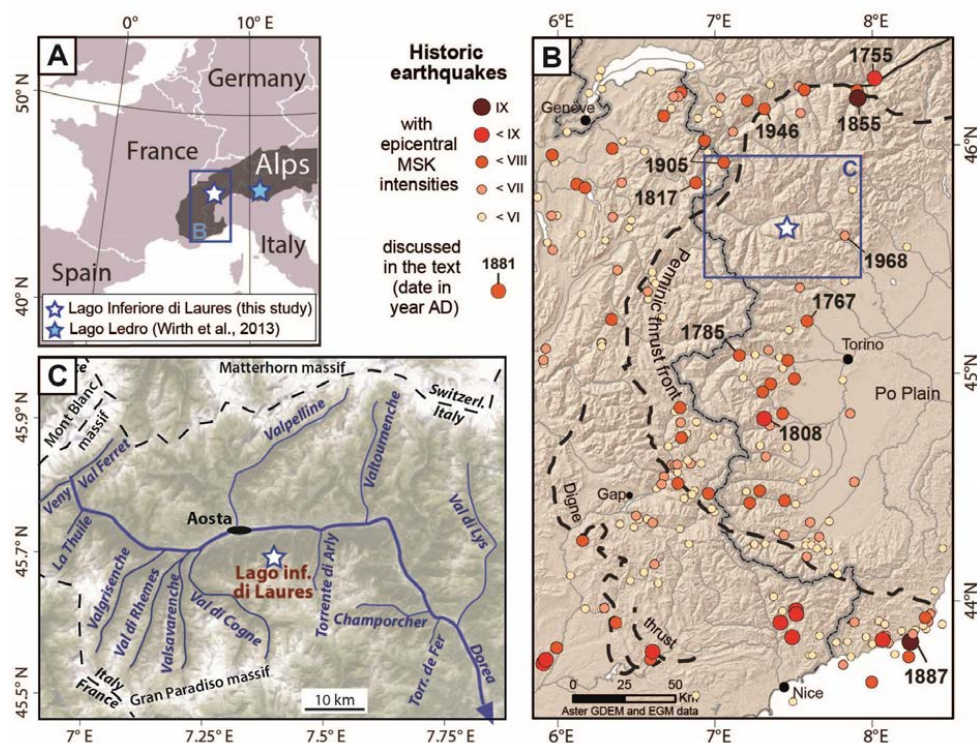
31 Natural hazards (e.g. earthquakes, floods, landslides, etc.) are of particular concern for societies as they cause
32 widespread loss of life, damage to infrastructure and economic deprivation (e.g. Munich Re Group, 2003). The
33 frequency of both geological (i.e. earthquakes) and hydrological (i.e. floods) events vary in time mainly as a
34 function of tectonic processes and climatic regimes, respectively. Such changes need to be taken into account for
35 robust risk assessments. This becomes even more crucial in the context of global warming, which is expected to



36 lead to a modification of the hydrological cycle and associated floods. However, available instrumental time-
37 series generally cover a short time span, precluding a comprehensive knowledge of the tectonic and climatic-
38 related variability. In this respect, historical and natural archives were widely studied to extend earthquake and
39 flood catalogues further back in time (e.g. Guidaboni et al., 2007; Rizza et al., 2011; Brázdil et al., 2012;
40 Ballesteros-Cánovas et al., 2015; Benito et al., 2015; Denniston et al., 2015; Ratzov et al., 2015). Among them,
41 lake sediments have been shown to be valuable archives as they record past events in a continuous and high-
42 resolution mode (e.g. Lauterbach et al., 2012; Wilhelm et al., 2012a; Strasser et al., 2013; Wirth et al., 2013;
43 Amman et al., 2015; Van Daele et al., 2015). The greater hydraulic energy of flooded rivers increases their
44 capacity to erode and transport sediments. Downstream, lakes may act as sediment traps, resulting in the
45 deposition of a coarser-grained layer that will be preserved in time (e.g. Gilli et al., 2013; Schillereff et al.,
46 2014). In case of earthquakes, ground shaking may disturb lake sediments by triggering co-seismic in situ
47 deformation or post-seismic deposits related to subaquatic mass movements of slope sediments and resuspension
48 (e.g. Avşar et al., 2014; Van Daele et al., 2015). Identification and dating of all 'event layers' in sediment cores
49 enable to reconstruct past event occurrences over century to millennia. Recently, some studies have also
50 developed methods to reconstruct magnitude of past events. Magnitude of past flood events may be
51 reconstructed through grain size (e.g. Schiefer et al., 2011; Lapointe et al., 2012; Wilhelm et al., 2015;
52 Schillereff et al., 2015) or through the total volume of sediments transported and deposited during the flood (e.g.
53 Jenny et al., 2014; Wilhelm et al., 2015). Reconstruction of past earthquake magnitudes is approached by
54 comparing regional records of seismic-induced deposits (e.g. Strasser et al., 2006; Wilhelm et al., 2016b) or
55 through the deposit's spatial extent and thickness (Moernaut et al., 2014).

56 The southern European Alps (Northern Italy) are particularly harmed by natural hazards such as floods and
57 earthquakes (e.g. Boschi et al., 2000; Guzetti and Tonelli, 2004; Eva et al., 2010), due to the proximity of both
58 the Mediterranean Sea and the seismically-active Alpine region. The Mediterranean Sea is the primary moisture
59 source for orographic precipitation on the southern flank of the Alps (e.g. Buzzi and Foschini, 2000; Lionello et
60 al., 2012). Spatially restricted convective and spatially more exhaustive cyclonic precipitation events may lead to
61 catastrophic floods (Gaume et al., 2009; Marchi et al., 2010), as it for instance occurred in October 2000 or June
62 1957 (Ratto et al., 2003). Moreover, the south-western European Alps is a seismogenic region that experienced
63 great earthquakes with macroseismic Medvedev-Sponheuer-Kárník (MSK) intensities up to IX and estimated
64 magnitudes higher than 6., e.g. the Ligurian earthquake in 1887 ($M_w = 6.8$; Larroque et al., 2012) and the Visp
65 earthquake in 1855 ($M_w = 6.2$; Fäh et al., 2011; Fig. 1),

66 In this context, the present study aims at exploring the potential of a lake sequence as recorder of past floods and
67 earthquakes in the western Italian Alps. This is undertaken by studying the high-elevation sediment sequence of
68 Lago Inferiore de Laures, Valle d' Aosta.



69

70 **Figure 1.** Location of Lago Inferiore de Laures in the Mediterranean Italian Alps (A), with locations of historical earthquakes
 71 with epicentral MSK intensity above IV (B). The earthquake catalog is provided by the database SisFrance
 72 (<http://infoterre.brgm.fr/>; Lambert and Levret-Albaret, 1996; Scotti et al., 2004). Location of Lago Inferiore de Laures
 73 catchment area in the hydrological network of Valle d'Aosta (C).

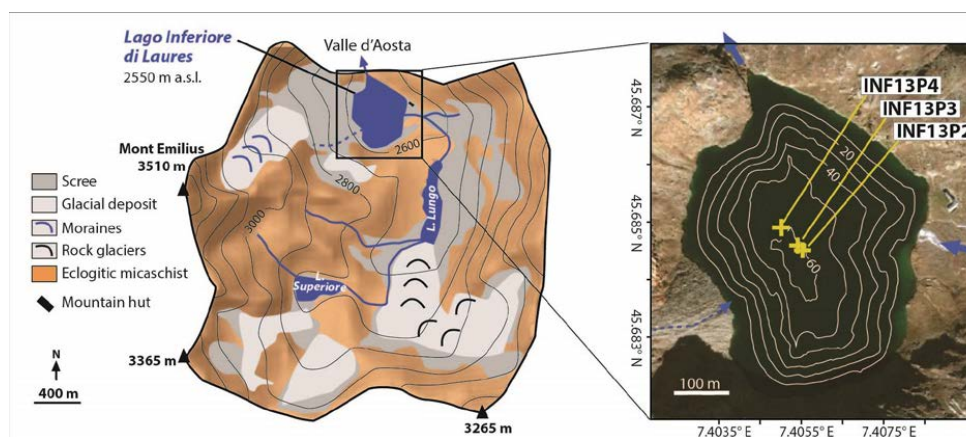
74

75 2. Study site

76 Valle d'Aosta is located at the foot of the Mont Blanc and Monte Rosa massifs, north to the vast Italian Po Plain,
 77 and ~180 km north of the Mediterranean Sea (Fig. 1). Lago Inferiore de Laures (2450 m a.s.l., 45°41'N, 7°24'E)
 78 is a small, high-elevation lake located on the north-facing slope of Valle d'Aosta (Fig. 1C). Due to the high
 79 elevation of the catchment, only the area surrounding the lake is covered by alpine meadow vegetation, which is
 80 impacted by grazing activity. Most of the catchment is covered by rock and scree. Rock is mainly made of
 81 eclogitic micaschist, which was eroded by small glaciers in the western and southern parts of the catchment as
 82 evidenced by the presence of glacial deposits and moraines (Fig. 2). These glaciers have disappeared and only a
 83 rock glacier is still active in the south-eastern part of the catchment. The catchment is mainly drained by the
 84 mountain stream that crosses Lago Superiore and Lago Lungo before entering Lago Inferiore. These two upper
 85 lakes act as two sediment traps and, thereby, all the upper part of the catchment does not contribute to the detrital
 86 inputs in Lago Inferiore. Detrital inputs are mainly provided by (i) the lower part of the main stream and its
 87 eastern tributary and by (ii) a temporary stream that drains glacial deposits west from the lake. This results in
 88 two distinct major detrital input sources to the lake, as suggested by the aerial and subaquatic deltas built on the



89 eastern and western lake shores. Mobilization of detrital material is restricted to summer months and beginning
90 of autumn (June/July to mid-November) when the lake ice cover is absent and catchment soils are thawed and
91 free of snow cover.
92



93
94 **Figure 2.** Geological and geomorphological characteristics of the Lago Inferiore de Laures catchment area (left panel).
95 Bathymetric map of Lago Inferiore de Laures and coring sites (right panel).

96

97 **3. Methods**

98 **3.1. Core description and logging**

99 In fall 2013, a bathymetric survey with a single-beam echosounder was carried out at Lago Inferiore and
100 revealed a narrow flat basin in the centre of the lake with a maximum water depth of 60.7 m (Fig. 2). Three up to
101 62 cm long gravity cores have been retrieved from the depocenter of the lake. The uppermost 13 cm of core
102 INF13P2 were disturbed during the coring. The three cores were split lengthwise and the visual macroscopic
103 features of each core were examined in detail to determine the different sedimentary facies. Based on these
104 facies, a stratigraphic correlation was carried out between the three cores to document the spatial extent and
105 succession of the different facies over the lake basin.

106 High-resolution images and gamma-ray attenuation bulk density (GRAPE) data were acquired on a Geotek™
107 multisensor core-logger (Institute of Geological Sciences, University of Bern). The bulk density is obtained at a
108 5-mm downcore resolution. X-Ray analyses on the core INF13P3 were carried out on an Itrax™ (Cox Analytical
109 Systems) X-ray fluorescence (XRF) core scanner (Institute of Geological Sciences, University of Bern), using a
110 Molybdenum tube, set to 30 kV, 35 mA with a 10-s count-time and a 1-mm sampling step. The scattered
111 incoherent (Compton) radiation of the X-ray tube (Mo_{inc}) varies with bulk element mass/sediment density
112 (Croudace et al., 2006) and, thereby, provides a high-resolution proxy for sediment density (e.g. Wilhelm et al.,
113 2016a). Mo_{inc} values were averaged at a 5-mm resolution for correlation with the GRAPE-density, which
114 resulted in a linear, positive, and significant correlation ($r=0.88$, $p<10^{-4}$). This allowed using Mo_{inc} as a proxy of
115 sediment density for identifying mm-scale event layers, e.g. flood and mass-movement deposits. Event layers are



116 characterized by higher density because of the high amount of detrital material provided in a short time (e.g.
117 Støren et al., 2010; Gilli et al., 2012; Wilhelm et al., 2012b).

118 Grain-size analyses were performed on core INF13P3 using a Malvern Mastersizer 2000 (Institute of Geography,
119 University of Bern) at a 5-mm continuous interval. Before the grain-size analysis, the samples have been treated
120 in a bath of diluted hydrogen peroxyde during 3 days to remove the organic matter. The disappearance of the
121 organic matter was checked through smear slide observations. Grain-size analyses of the detrital material were
122 performed to characterize the transport-deposition dynamics of the deposits (e.g. Passega, 1964; Wilhelm et al.,
123 2013; 2015).

124

125 **3.2. Dating methods**

126 To date the lake sequence over the last century, short-lived radionuclides (^{226}Ra , ^{210}Pb , ^{137}Cs) were measured by
127 gamma spectrometry at EAWAG (Dübendorf, Switzerland). The core INF13P3 was sampled following a non-
128 regular step of 1 ± 0.2 cm, matching the facies boundaries. The ^{137}Cs measurements generally allow two main
129 chronostratigraphic markers to be located: the fallout of ^{137}Cs from atmospheric nuclear weapon tests
130 culminating in AD 1963 and the fallout of ^{137}Cs from the Chernobyl accident in AD 1986 (Appleby, 1991).
131 ^{226}Ra is measured as a proxy for the supported ^{210}Pb in order to calculate the unsupported ^{210}Pb that corresponds
132 to the excess ^{210}Pb (e.g. Schmidt et al., 2014). The decrease in excess ^{210}Pb ($^{210}\text{Pb}_{\text{ex}}$) and the Constant
133 Flux/Constant Sedimentation (CFCS) model allow a mean sedimentation rate to be calculated (Goldberg, 1963).
134 The standard error of the linear regression of the CFCS model is used to assess the uncertainty of the
135 sedimentation rate. The ^{137}Cs chronostratigraphic markers are then used to control the validity of the ^{210}Pb -based
136 sedimentation rate.

137 In addition to short-lived radionuclides, historical lead (Pb) contaminations were also used to control the ^{210}Pb -
138 based chronology (e.g. Renberg et al. 2001). In order to identify lead contamination, we used the geochemical
139 measurements carried out on the ItraxTM XRF core scanner on core INF13P3. Pb intensities were normalized to a
140 well-measured detrital element, i.e. the titanium (Ti), to disentangle natural and human-induced changes in Pb.
141 Recorded Pb variations were compared to historical lead emissions in Switzerland (Weiss et al., 1999), the
142 closest place to the studied site where lead emissions are well documented.

143

144 **4. Results**

145

146 **4.1. Description of the sedimentary deposits**

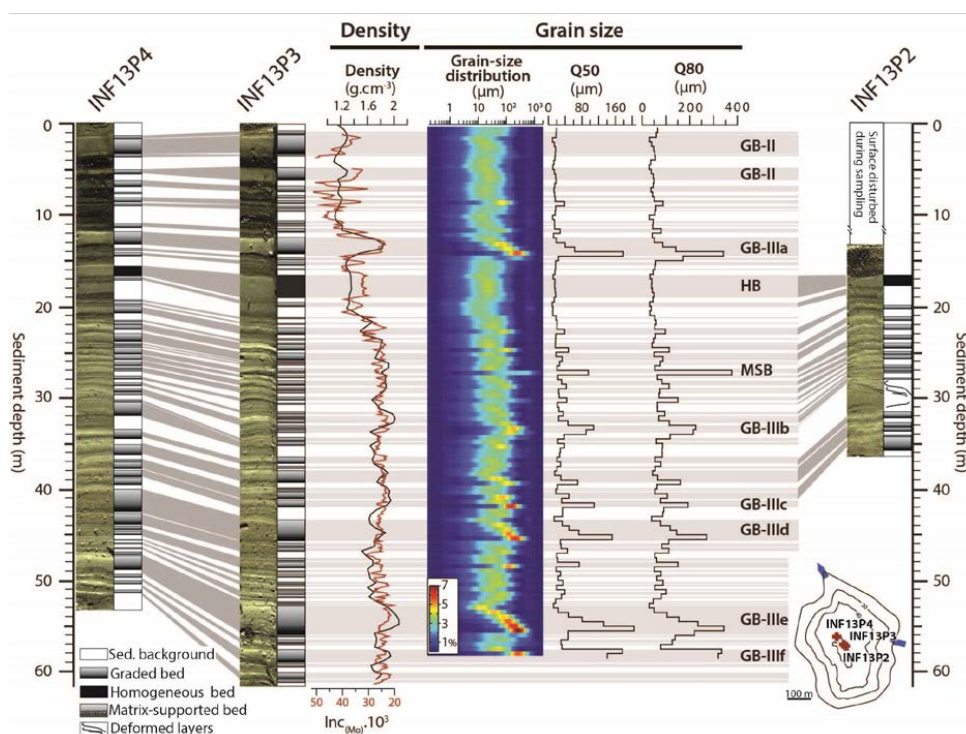
147 The sediment consists of a finely bedded, greenish brown mud mainly composed of detrital material with grain-
148 sizes in the silt-clay fraction and amorphous organic matter. Smear-slide observations reveal that the organic
149 matter content increases upcore, concurrently to the dark brown colour of these deposits (Fig. 3). These fine-
150 grained deposits representing the background hemi-pelagic sedimentation, are interrupted by 77 beds
151 characterized by rather coarse material, lower organic matter content, and higher density. According to several
152 studies providing a comprehensive overview of event layers (e.g., Mulder and Cochonat, 1996; Gani, 2004;
153 Wilhelm et al., 2015; Van Daele et al., 2015), the 77 beds represent short-term depositional events and they



154 correspond to 74 graded beds (GBs), 1 matrix-supported bed (MSB), 1 homogeneous bed (HB) and 1 deformed
 155 layer (Fig. 3).

156 The 74 GBs are all characterized by a sharp and coarse-grained base, a fining-upward trend and a thin, whitish
 157 fine-grained capping layer. There is no evidence for erosive bases. The stratigraphic correlation reveals that
 158 almost all GBs appear in the three cores. Only four GBs identified in cores INF13P3 (33.3-35 cm) and INF13P4
 159 (29.6-32 cm) are missing in core INF13P2. In core INF13P2, the four missing GBs stratigraphically correspond
 160 to a deformed layer (28-30 cm; Fig. 3).

161



162

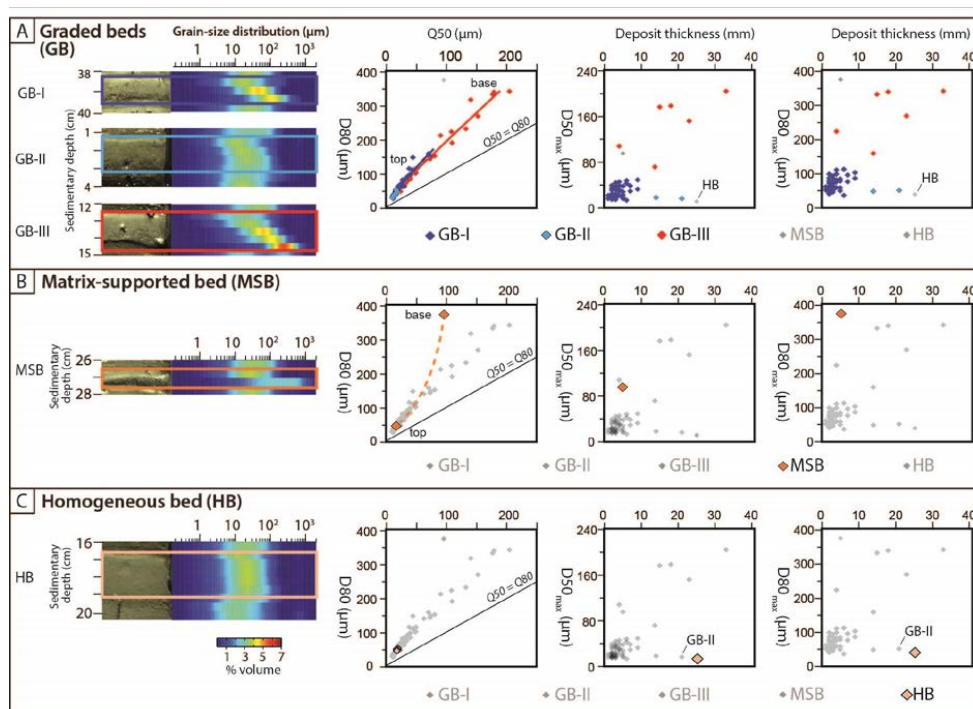
163 **Figure 3.** Lithological descriptions of cores and stratigraphic correlations based on sedimentary facies. Variability in grain-
 164 size distribution is shown for the core INF13P3. The density measurements performed by gamma-ray attenuation are shown
 165 close to Mo_{inc} , used as a high-resolution density proxy.

166

167 The Passega-type (D50 vs. D80) diagram highlights a steady decrease of both the median (D50) and the coarse
 168 percentile (D80) from the base to the top of the GBs (Fig. 4A). This confirms the visually-identified fining-
 169 upward trend of all GBs. 'D50_{max} vs. deposit thickness' and 'D80_{max} vs. deposit thickness' diagrams (where
 170 D50_{max} and D80_{max} are defined as the highest value of D50 and D80 of each GB) suggest that the 74 GBs may be
 171 differentiated in 3 types (Fig. 4A). Most of the GBs (66 of 74) form a well-grouped cluster characterized by low
 172 values of thickness (1 - 10 mm), D50_{max} (10 - 50 μ m) and D80_{max} (35 - 115 μ m). These 66 GBs are labelled GB-I
 173 (dark blue points, Fig 4A). These diagrams highlight 2 GBs, labelled GB-II (light blue points, Fig. 4A), also



174 characterized by a very fine grain size ($D_{50_{max}}$ of 16-18 μm and $D_{80_{max}}$ of 50-52 μm) but a larger thickness (14-
 175 21 mm) than GB-I. In contrast, some GBs (6 of 74; labelled GB-III; red points, Fig. 4A) are scattered in the
 176 'percentile vs. thickness' diagrams but well distinguishable from GB-I and GB-II because of both their coarser
 177 grain size (D_{50} of 70 - 200 μm and D_{80} of 160 - 350 μm) and larger thickness (from 3 to 33 mm). The distinct
 178 characteristics of the three GB types suggest distinct dynamics of sediment transport and deposition and, thereby,
 179 distinct triggers (discussed in sections 5.1.1. and 5.2.1.).



180
 181 **Figure 4.** Close-eye views of event layers (left) and their positions in a Passega-type (Q_{50} vs. Q_{80}) diagram as well as in
 182 'percentile vs. deposit thickness' diagrams (right) for the graded beds (A), the matrix-supported bed (B) and the homogenous
 183 bed (C).

184
 185 The MSB identified at 27 cm in core INF13P3 differs from the GBs by the poorly sorted fining-upward trend
 186 (Fig. 3 and 4B). This is well highlighted in the Passega-type diagram where the pattern is almost vertical,
 187 describing a large decrease of the coarse percentile (D_{80}) without noticeable median (D_{50}) variation. The 2.5
 188 mm-thick HB identified at 17 cm in core INF13P3 is characterized by a sharp base, a thin, whitish fine-grained
 189 capping layer and a central part with a fine and perfectly homogeneous grain size (Fig. 3 and 4C).

190 A 3.5 cm-thick layer at 28 cm in core INF13P2 is characterized by mixed beds in the lower part and folded beds
 191 in the upper part (Fig. 3). The stratigraphic correlation reveals that this deformed layer is overlain by a thin
 192 graded bed that becomes much thicker in cores INF13P3 and INF13P4. In core INF13P3, this graded bed

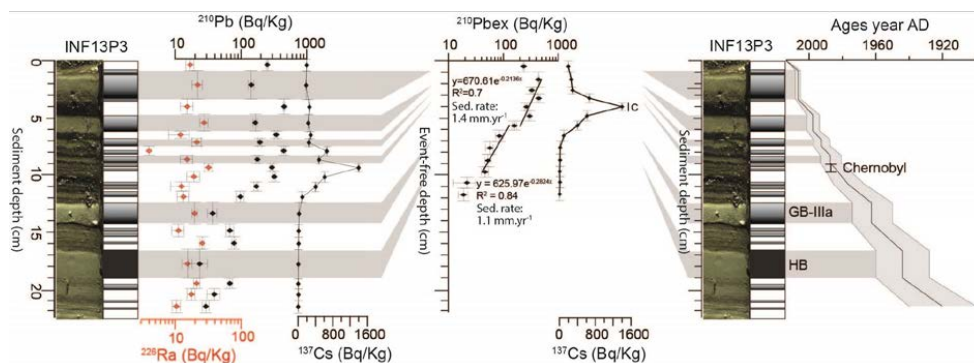


193 corresponds to a GB-III (labelled GB-IIIb in Fig. 3). In addition, the stratigraphic correlation suggests that this
194 deformed layer is not intercalated in the sediment sequence (e.g. slump) but corresponds to in situ deformation.

195

196 4.2. Chronology

197 The excess ^{210}Pb ($^{210}\text{Pb}_{\text{ex}}$) profile in cores INF13P3 shows a steady decrease in activity from 436 to 11 Bq/kg.
198 The profile is, however, punctuated by depths with very low values, which correspond to thick event layers (Fig.
199 5). We excluded $^{210}\text{Pb}_{\text{ex}}$ values associated with these instantaneous deposits to construct a synthetic sediment
200 record (Arnaud et al., 2002). The CFCS model (Goldberg, 1963) was applied to the synthetic $^{210}\text{Pb}_{\text{ex}}$ profile and
201 indicates that the sequence is characterized by two periods of different sedimentation rates (SR). SR shifts from
202 $1.1 \pm 0.2 \text{ mm.yr}^{-1}$ in the lower portion of the core to $1.4 \pm 0.36 \text{ mm.yr}^{-1}$ in the topmost 5.5 cm. The CFCS model-
203 derived ages were used to develop continuous age-depth relationships for core INF13P3 (Fig. 5). A synthetic
204 ^{137}Cs profile was built and displays a progressive increase until a peak of 1400 Bq.kg^{-1} at 9.5 cm (Fig. 5). Such
205 high ^{137}Cs values are unequivocal of the fallout associated to the 1986 Chernobyl accident in the region (e.g.
206 Vanni re et al., 2013; Wilhelm et al., 2015; 2016). The second expected peak related to the nuclear weapon tests
207 in AD 1963 cannot as clearly defined. It might be diluted in the very high ‘‘Chernobyl’’ signal.



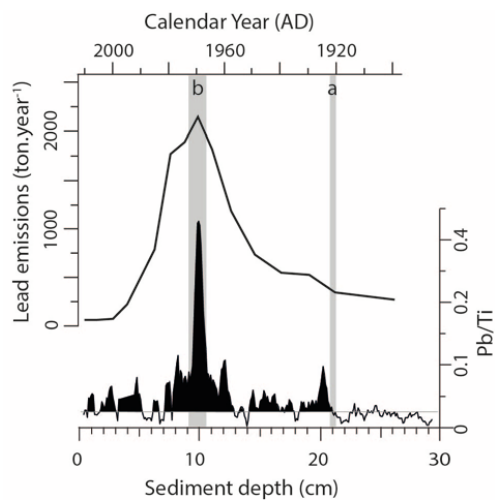
208

209 **Figure 5.** ^{226}Ra , ^{210}Pb and ^{137}Cs profiles for core INF13P3 (left). Application of a CFCS model to the event-free sedimentary
210 profile of $^{210}\text{Pb}_{\text{ex}}$. Resulting age–depth relationship with 1σ uncertainties and locations of the historic ^{137}Cs peak of
211 Chernobyl (AD 1986) supporting the ^{210}Pb -based ages.

212

213 The Pb/Ti ratio shows a low background (≤ 0.5) in the lower part of core INF13P3 (Fig. 6). At 21 cm, the Pb/Ti
214 ratio increases and remains almost always above 0.5 upcore. From 13 to 8 cm, it reaches high values (> 1) with a
215 maximum at 10 cm (> 4). These distinct steps well mirrors historical Pb emissions in Switzerland with low
216 emissions ($< 500 \text{ tons.year}^{-1}$) until AD 1920 and high emissions ($> 1000 \text{ tons.year}^{-1}$) from the 1950s to the
217 1980s, with a maximum around 1970 (Weiss et al., 1999). The increase of Pb emission in the 1920s may
218 correspond to the beginning of the use of leaded gasoline and the peak in Pb emission (1970s) to its maximal use
219 (Weiss et al., 1999; Arnaud et al., 2004). These two steps in historical Pb contaminations, well-marked in the
220 Pb/Ti ratio, may thus be used as additional chronological markers. The good agreement between these two
221 chronological markers and the ^{210}Pb -derived ages supports the validity of our age–depth model (Fig. 7).

222



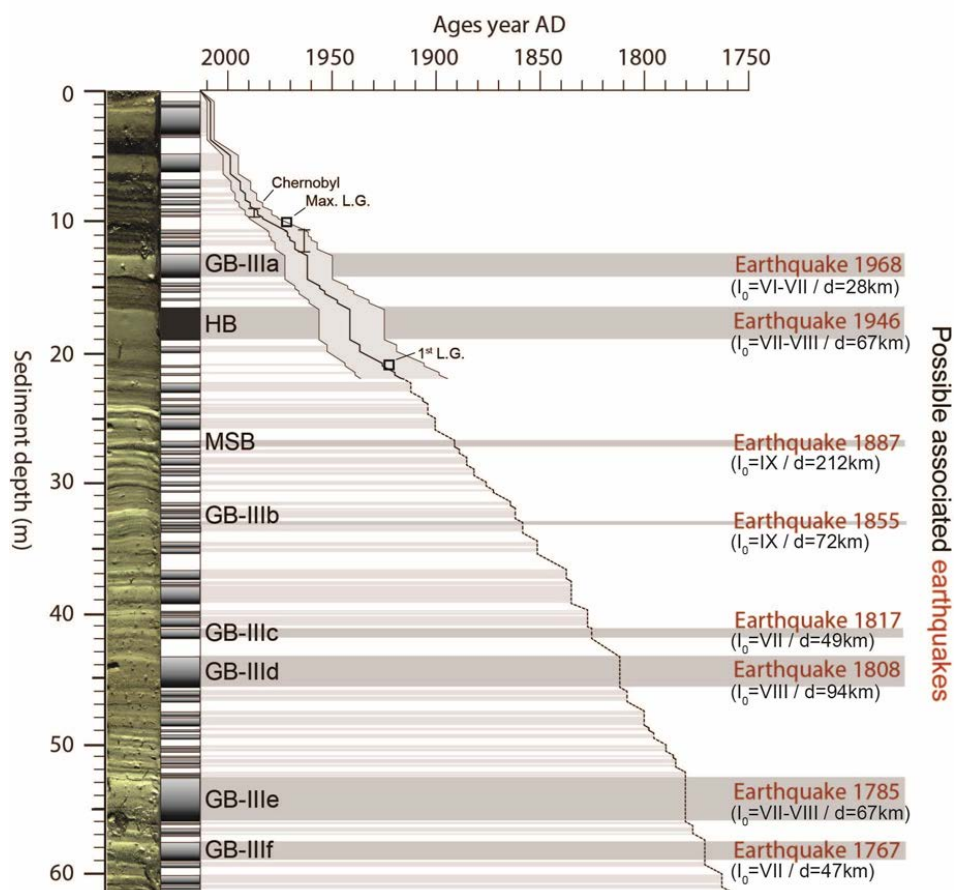
223

224 **Figure 6.** Historical lead (Pb) emissions in Switzerland (from Weiss et al., 1999) compared to the Pb/Ti ratio measured in
225 core INF13P3.

226

227 Overall, the good chronological agreement between these independent markers and the ^{210}Pb -derived ages
228 supports the validity of our age-depth model (Fig. 6). The extrapolation of the CFCS model-derived ages suggest
229 that core INF13P3 covers the ~270 years (Fig. 7).

230



231

232 **Figure 7.** Age–depth relationship of core INF13P3 based on the ^{210}Pb -based sedimentation rate (with 1σ uncertainties) for
 233 the last century and based on the extrapolation of this sedimentation rate for the lower part of the core. The three
 234 chronological markers supporting the ^{210}Pb -based sedimentation are shown: the ^{137}Cs peak associated to the Chernobyl
 235 accident (AD 1986), the first use of leaded gasoline (1920s) and its maximal use (1970s). Labels (GB-III, HB and MSB)
 236 correspond to the mass-movement-induced deposits. Historical earthquakes, possibly associated to these mass-movement-
 237 induced deposits, are indicated.

238

239 5. Discussion

240

241 5.1. Lago Inferiore de Laures sediments: a record of past earthquakes?

242 5.1.1. Trigger of MSB, HB, GB-III and the deformed layer

243 The MSB pattern in the Passega-type diagram suggests that the transport energy is supplied by the sediment
 244 weight rather than by a water current velocity, i.e. formation of concentrated density flows of suspended



245 sediments during a sub-aquatic mass movement (e.g. Mulder et Cochonnat, 1996; Arnaud et al., 2002; Wilhelm
246 et al., 2016b).

247 The HB characteristics are very similar to deposits previously described by many studies (e.g. Schnellmann et al.
248 2005; Beck 2009, Petersen et al., 2014). These studies proposed that a sub-aquatic mass movement triggers the
249 oscillation of the whole lake water body (i.e. seiche), which homogenizes the sediment put in suspension by
250 either the water oscillation or the mass movement. Therefore, HB most probably results also from a mass
251 movement.

252 GBs are associated with turbidity currents triggered by either flood events or mass movements (e.g. Sturm and
253 Matter, 1978; Shiki et al., 2000; Arnaud et al., 2002; Mulder and Chapron, 2011; Wilhelm et al., 2012b). In the
254 latter case, they are formed by the sediment that is transported in suspension during the mass movement and then
255 deposited over the mass-wasting deposits and/or further in the lake basin (e.g. Shiki et al., 2000; Schnellmann et
256 al., 2005). These mass-movement-induced GBs are also known to be generally thicker than those induced by
257 flood events because mass movements may mobilize much larger quantities of sediments than floods (e.g. Shiki
258 et al., 2000; Schnellmann et al., 2005; Fanetti et al., 2008; Wilhelm et al., 2013). Accordingly, the rare GB-III
259 characterized by large thicknesses may be associated to mass movements. The position of GB-IIIb on top of the
260 deformed layer (Fig. 3) further supports this assumption because (i) the immediate stratigraphic succession
261 suggests a common trigger for these two deposits and because of (ii) the ability of strong earthquake shaking to
262 trigger (co-seismic) in situ deformation and (post-seismic) mass movements.

263 Folded and mixed beds of the deformed layer are similar characteristics to the so-called “mixed layers” that
264 result from shear stress applied to poorly consolidated sediments during strong earthquake shaking (e.g. Marco et
265 al., 1996; Rodriguez-Pascua et al., 2000; Migowski et al., 2004; Monecke et al., 2004). Accordingly, the
266 deformed layer is interpreted as the result of a strong earthquake.

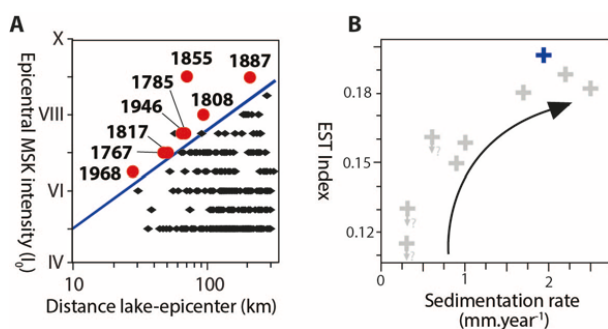
267

268 **5.1.2. Chronological control on the mass-movement-induced layers**

269 Mass movements can be triggered by spontaneous failures due to overloading of slope sediments, snow
270 avalanches, fluctuations in lake levels, rockfalls, or earthquakes (e.g., Van Daele et al., 2015; Wilhelm et al.,
271 2016b). Here changes of lake level can be excluded because the water level of Lago Inferiore is well controlled
272 by a bedrock outlet. Rockfalls seem also unlikely as there is no geomorphological evidence of major rockfalls in
273 the catchment. Earthquakes are known to affect the region and may thus be a good candidate. In addition, the
274 earthquake trigger is the only candidate to explain the in situ deformed layer with associated GB-IIIc. To test the
275 earthquake trigger of all mass-movement-induced layers (i.e. GB-III, HB and MSB), their ages are compared to
276 the dates of historical earthquakes well documented over the last centuries (database SisFrance,
277 <http://www.sisfrance.net>; Lambert and Levret-Albaret, 1996; Scotti et al., 2004 and database CFTI4Med,
278 <http://storing.ingv.it/cfti4med/>, Guidoboni et al., 2007). GB-IIIa and HB are respectively dated to AD 1962 ±12
279 and 1941 ±16 years (Fig. 5). These dates corresponds well to two strong (epicentral MSK intensity up to VIII)
280 and close (max. 70 km) historical earthquakes occurring in AD 1968 and 1946 (Figs. 1 and 7). The extrapolation
281 of the ²¹⁰Pb-based sedimentation rate allows estimating ages of the older mass-movement-induced layers to AD
282 1891, 1859, 1826, 1811, 1780 and 1771, respectively (Fig. 7). All of them correspond well to relatively strong



283 and/or close earthquakes in AD 1887, 1855, 1817, 1808, 1785 and 1755, respectively. Age differences between
284 deposits and associated historical earthquakes are lower than 5 years, except between GB-IIIc dated to AD 1826
285 and the AD 1817 Chamonix earthquake. Moreover, the AD 1855 earthquake appears to be both stronger and
286 closer than other historical earthquakes (Fig. 8), suggesting that it generated the strongest shaking at the lake site.
287 This corresponds well to the associated in situ deformed layer that requires strong earthquake shaking to be
288 formed. Overall, this good temporal agreement highly supports that mass-movement-induced layers may have
289 been triggered by historical earthquakes.



290

291 **Figure 8.** (A) Diagram “distance of earthquakes to the lake vs. epicentral MSK intensity” that aims at confirming that the
292 earthquakes associated to the mass-movement-induced deposits are the strongest and/or the closest to the lake. Black crosses
293 indicate all historic earthquakes closer than 120 km to the lakes with epicentral MSK intensities \geq IV. Red dots with dates
294 correspond to historical earthquakes associated to the mass-movement-induced deposits in Figure 7. The sensitivity threshold
295 (blue line) is placed to delimit the recorded from the non-recorded earthquakes. (B) The ‘Earthquake Sensitivity Threshold
296 Index’ (ESTI) is compared to the sedimentation rate for Lago Inferiore de Laures (blue cross) and other similar Alpine lakes
297 (grey crosses) studied by Wilhelm et al. (2016b). Arrows show that these ESTIs are maximum values.

298

299 5.1.3. Earthquake record and lake sensitivity

300 The recorded earthquakes are expected to be the strongest and/or the closest to the lake, as those are expected to
301 have generated the largest ground motions in the lake area. Thereby, they should appear in the upper left corner
302 of a ‘distance vs. epicentral MSK intensity’ diagram (e.g. Monecke et al., 2004; Wilhelm et al., 2016b). This is
303 exactly what we observe when all historical earthquakes are plotted in such a diagram (Fig. 8A), supporting the
304 temporal assignment of the mass movements to the earthquakes.

305 The record of eight earthquakes over ~270 years (i.e. return period of ~35 years) suggests a high sensitivity of
306 Lago Inferiore de Laures to earthquake shaking, as such a high frequency of earthquake-induced deposits has
307 rarely been observed in the region (e.g. Guyard et al., 2007; Lauterbach et al., 2012; Simonneau et al., 2013;
308 Strasser et al., 2013; Kremer et al., 2015; Chapron et al., 2016; Wilhelm et al., 2016b). To quantify and compare
309 its sensitivity to other lakes, an empirical threshold line was defined that limits the domains of the recorded from
310 the non-recorded earthquakes (blue line in Fig. 8A). The slope ($a=1,08$) of this sensitivity threshold appeared
311 very similar to those defined for five other Alpine lakes ($a=1,13$ in Wilhelm et al., 2016b). This suggests a
312 relatively uniform attenuation of the seismic waves in the western Alps. In addition, this allows a direct
313 comparison of sensitivity with these other lakes through the ‘Earthquake Sensitivity Threshold Index’ (ESTI).



314 ESTI was defined as the inverse of the intercept of the threshold line with the intensity axis at 10 km from the
315 lake (Wilhelm et al., 2016b). The ESTI score for Lago Inferiore reaches 1.9, i.e. the highest value of the Alpine
316 lakes for which the sensitivity was quantified (Fig. 8B). This high sensitivity of Lago Inferiore to earthquake
317 shaking may be explained by many factors like slope angle, sediment thickness or geotechnical properties of the
318 sedimentary succession (e.g., Morgenstern, 1967; Strasser et al., 2011; Ai et al., 2014; Wiemer et al., 2015).
319 However, Wilhelm et al. (2016b) suggested that the dominant factor explaining the lake sensitivity of such
320 Alpine lakes is the sedimentation rate, i.e. that the lake sensitivity increases when the sedimentation rate
321 increases, which is in agreement with the lake's high sedimentation rate (Fig. 8B).

322

323 **5.2. Lago Inferiore de Laures sediments: a record of past floods?**

324 **5.2.1. Trigger of GB-I and GB-II**

325 The high frequency of GB-I (66 deposits over 270 years, return period of ~4 years) makes it unlikely that these
326 layers were the result of mass movements. In addition, the very uniform values of grain size and thickness
327 characterizing GB-I suggest that they are triggered by processes where sediment erosion, transport and
328 deposition are well controlled/regulated. Many studies suggested that the amount and grain size of eroded,
329 transported and deposited material in case of flood events are controlled by the river discharge (e.g. Schiefer et
330 al., 2011; Lapointe et al., 2012; Jenny et al., 2014; Wilhelm et al., 2015). Therefore, flood processes seem to be
331 the best candidate to trigger GB-I.

332 The presence of grading in GB-II and their isolated positions in the 'percentile vs. thickness' diagram are similar
333 characteristics to GB-III, suggesting a common trigger for both GB-II and GB-III, i.e. mass movements. The two
334 GB-II are dated to AD 2006 \pm 2 and 1997 \pm 4 yrs., respectively (Fig. 5). An earthquake trigger is very unlikely as
335 no strong and/or close earthquake occurred at that time. A mass-movement trigger can, however, not be
336 excluded. Alternatively, Giguet-Covex et al. (2011) suggested that thickness of flood-induced GBs may
337 significantly increase without changes in grain size when human impact, i.e. grazing pressure in such high-
338 elevation catchments, became high. Sheep grazing and trampling would accelerate the mechanical soil
339 degradation, making erosion processes higher during floods. In this way, GB-II may also be triggered by floods
340 at time of high grazing activity, which currently occurs close to the lake as evidenced by the sheep pen located
341 on the shoreline of Lago Inferiore. In addition, these deposits appear in the uppermost part of the cores
342 characterized by high organic matter content. This higher content of lacustrine organic matter might result from a
343 higher primary production linked to an increase of nutrients inputs with the higher grazing activity.

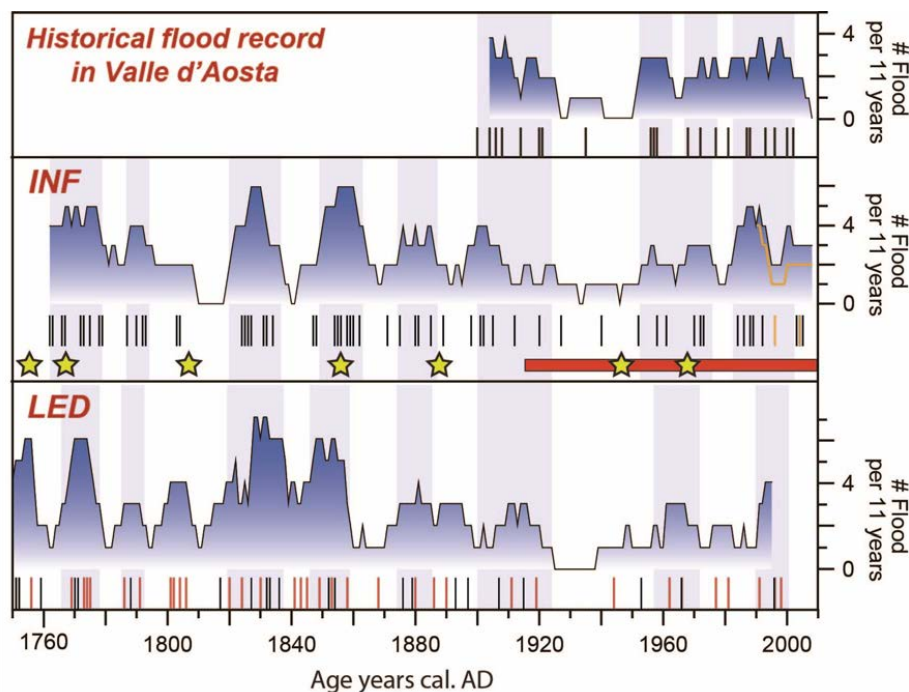
344

345 **5.2.2. Chronological control on flood-induced deposits**

346 The assignment of a flood trigger to GB-I and GB-II may be assessed by using historical flood data. A direct
347 comparison between deposit ages and historical flood dates is precluded because the outlet stream of Lago
348 Inferiore does not flow through any village downstream. Instead, the frequency of GB-I and GB-II occurrences
349 was compared to the frequency of historical summer-autumn floods that affected streams and villages around
350 Lago Inferiore as documented by Mercalli et al., 2003. For the comparison, a historical flood event that occurred
351 in mid-May was not considered as we assume that the lake was frozen at that time. Over the last century,



352 historical data reveal a high flood frequency (up to 4 floods per 11 years) during periods AD 1900-1920 and AD
353 1950-2010 and a low frequency (less than 1 flood per 11 years) during the period AD 1920-1950 (Fig. 9). This
354 multi-decennial variability in flood frequency is well reproduced by the sediment record when considering both
355 GB-I and GB-II. Indeed, both the three time periods and the range of flood-frequency values (from 1 to 4 per 11
356 years) are very similar between records. If GB-II are removed from the sediment record, the reconstructed flood
357 frequency shows a decrease more pronounced over the last decades (orange line in Fig. 9) than in the historical
358 record. This may support a flood trigger (during a period of high grazing activity) for GB-II. Overall, the good
359 agreement with the historical data, when considering both GB-I and GB-II, supports that Lago Inferiore
360 sediments record well the decennial variability of past floods.
361



362
363 **Figure 9.** Comparison of the reconstructed Lago Inferiore de Laures flood frequency (11-years running sum) with the
364 frequency (11-years running sum) of historical floods in Aosta Valley (Mercalli et al., 2003) and the frequency of summer-
365 autumn floods recorded in Lago di Ledro (Wirth et al., 2013). Vertical bars correspond to flood occurrences. For Lago
366 Inferiore de Laures, the two orange vertical bars correspond to the GB-II. The orange curve corresponds to the flood
367 frequency when these two deposits are not considered. Yellow stars correspond to the earthquake-induced deposits indicated
368 as chronological markers. For Lago di Ledro record, black vertical bars correspond to summer floods and red vertical bars to
369 autumn floods.

370



371 **5.2.3. Paleoflood record in the regional climatic setting**

372 Historical data revealed that flood events mostly occurred in summer and autumn (20 of 21), i.e. during the ice-
373 free season of the lake. Thereby, the flood activity recorded in Lago Inferiore sediments well represents the
374 variability of floods that impacted communities in Valle d'Aosta. Among these events, 5 occurred in summer
375 and early autumn and affected localized area (i.e. only one mountain stream, Mercalli et al., 2003). According to
376 the season and their limited spatial extent, these events are most probably triggered by local convective events,
377 i.e. thunderstorms. The 15 other events occurred equally in summer and autumn and affected many tributaries
378 and/or the main Dora Baltea River. As these events affected large catchments (ca. 200-2000 km²), they are most
379 probably related to mesoscale convective events typical of the Mediterranean climate. Thereby, the flood activity
380 recorded in Lago Inferiore sediments is mainly related to large scale hydro-meteorological events and may
381 represent a 'regional' signal of the past summer-autumn flood variability. As these mesoscale events are formed
382 by humid air masses from the Mediterranean that flow northward through the Po Plain until the Alps, they may
383 also trigger floods in many Alpine regions located north to the Po Plain.

384 To test the 'regional' character of the reconstructed flood signal, the Lago Inferiore de Laures flood record was
385 compared to the Lago di Ledro flood record. Lago di Ledro is a low-elevation lake (660 m a.s.l.) located 280 km
386 east from Lago Inferiore de Laures, in the eastern part of the Alpine region located north to the Po Plain (Fig. 1).
387 Floods in Ledro catchment (111 km²) also occur mainly in summer and autumn due to mesoscale convective
388 events (Wirth et al., 2013). The extrapolation of the sedimentation rate enables to extend the centennial Lago
389 Inferiore de Laures flood record to the last 270 years (Fig. 7). From the comparison with the Lago di Ledro flood
390 record (Fig. 9), we observe that the range of flood-frequency values is in agreement between the two records, i.e.
391 between 0 and 6 floods per 11 years. Secondly, we observe strong similarities in the two flood records with
392 periods of low flood frequency in AD 1760-1780, 1785-1795, 1820-1835, 1875-1885, 1955-1975 and after 1990
393 and periods of low flood frequency in AD 1780-1785, 1810-1820, 1860-1875 and 1925-1955. However, some
394 discrepancies between the two records can be noticed around AD 1800, 1890-1920 and 1980-1990. They may be
395 related to localized events, e.g. thunderstorms, which may have different spatial and temporal dynamics between
396 sites. Overall, there is a good agreement in the main trends of the flood frequencies, suggesting that the two
397 flood records dominantly represent the decennial variability of mesoscale convective events triggering floods in
398 this part of the Mediterranean Alps.

399

400 **6. Conclusion**

401 The high-resolution sedimentological study of Lago Inferiore de Laures revealed 77 event layers over the last ca.
402 270 years. A detailed analysis suggested that 9 of 77 event layers are related to 8 mass-movements, while 66 of
403 77 are most probably related to flood events. The trigger of 2 event layers (those labelled GB-II) still remains
404 uncertain. The temporal assignment suggests a flood trigger during a period of high grazing activity. However,
405 further work is still required to confirm this hypothesis, e.g. by studying proxy of grazing activity like
406 coprophilous fungal ascospores (e.g. Davis and Schafer, 2006; Etienne et al., 2013).

407 The 8 mass movements were chronologically compared to the well documented historical seismicity. The
408 comparison revealed that mass movements in Lago Inferiore de Laures are most probably triggered by strong
409 (epicentral MSK intensity of VI-IX) and/or close (distance to the lake of 25-120 km) earthquakes. Compared to



410 other Alpine lakes, the high frequency of earthquake-induced mass movements (8 over ca. 270 years) suggested
411 a high sensitivity of Lago Inferiore de Laures sediments to earthquake shaking. Indeed, this lake is regionally the
412 most sensitive with an ESTI value of 1.9. In line with Wilhelm et al. (2016b), its high sedimentation rate may
413 explain this high sensitivity.

414 The frequency of flood-induced deposits was compared to the frequency of historical summer-autumn floods
415 that affected mountain streams and rivers in Valle d'Aosta. This showed that the (multi-)decennial frequency of
416 flood events that impacted local populations is well reproduced by the sedimentary record. The comparison with
417 the flood record of Lago di Ledro (Wirth et al., 2013), located 280 km east, suggested that the main trends of the
418 (multi-) decennial flood variability are in good agreement between records, suggesting a 'regional' character of
419 the two reconstructed flood signals linked to the typical Mediterranean mesoscale precipitation events.

420 Hence, this study showed that Lago Inferiore de Laures sediments seem to be a remarkable record of earthquakes
421 and floods, both natural hazards harming populations of this Alpine region. This should encourage further study
422 to extend the Lago Inferiore de Laures record further back in time. Such a long-term record of natural hazards
423 would improve our knowledge on the natural hazard occurrence and, thereby, enabling a better risk assessment.

424

425 **Acknowledgments**

426 B. Wilhelm's post-doctoral fellowship (2013-2014) was supported by a grant from the AXA Research Fund. We
427 would also like to thank Pierre Sabatier for his help to interpret the ^{210}Pb data.

428

429 **References**

430 Ai, F., M. Strasser, B. Preu, T. J. J. Hanebuth, S. Krastel, and Kopf A.: New constraints on the oceanographic vs. seismic
431 control on submarine landslides initiation: A geotechnical approach off Uruguay and northern Argentina, *Geo Mar.*
432 *Lett.*, 34(5), 399–417, 2014.

433 Amann, B., S. Sönke, and Grosjean, M.: A millennial-long record of warm season precipitation and flood frequency for the
434 Northwestern Alps inferred from varved lake sediments: implications for the future, *Quaternary Sci. Rev.*, 115, 89–100,
435 2015.

436 Appleby, P. G., N. Richardson and Nolan, P. J.: ^{241}Am dating of lake sediments, *Hydrobiologia*, 214, 35–42, 1991.

437 Arnaud, F., V. Lignier, M. Revel, M. Desmet, M. Pourchet, C. Beck, F. Charlet, A. Trentesaux, and Tribovillard N.: Flood
438 and earthquake disturbance of ^{210}Pb geochronology (Lake Anterne, North French Alps), *Terra Nova*, 14, 225–232,
439 2002.

440 Arnaud, F., M. Revel-Rolland, D. Bosch, T. Winiarski, E. Chapron, M. Desmet, N. Tribovillard, and N. Givélet: A reliable
441 300 years-long history of lead contamination in Northern French Alps from distant lake sediment records, *J. Environ.*
442 *Monit.*, 6(5), 448–456, 2004.

443 Avşar, U., A. Hubert-Ferrari, M. De Batist, G. Lepoint, S. Schmidt, and N. Fagel: Seismically-triggered organic-rich layers in
444 recent sediments from Göllüköy Lake (North Anatolian Fault, Turkey), *Quat. Sci. Rev.*, 103, 67–80, 2014.

445 Ballesteros-Cánovas J.A., Stoffel M., St George S., Hirschboeck K.: A review of flood records from tree rings. *Progress in*
446 *Physical Geography*, 39(6) 794–816, 2015.



- 447 Beck, C.: Late Quaternary lacustrine paleo-seismic archives in north-western Alps: Examples of earthquake-origin
448 assessment of sedimentary disturbances, *Earth Sci. Rev.*, 96(4), 327–344, 2009.
- 449 Benito G., Macklin M.G., Panin A., Rossato S., Fontana A., Jones A.F., Machado M.J., Matlakhova E., Mozzi P., Zielhofer
450 C.: Recurring flood distribution patterns related to short-term Holocene climatic variability. *Science reports* 5, 1-8,
451 2015.
- 452 Boschi E., Guidoboni, E., Ferrari, G., Mariotti, D., Valensise, G. and P. Gasperini: Catalogue of Strong Italian Earthquakes,
453 *Ann. Geofis.*, 43 (4), 268, 2000.
- 454 Brázdil, R., Kundzewicz, Z. W., Benito, G., Demarée, G., Macdonald, N., and Roald, L. A.: Historical floods in Europe in
455 the past Millennium, in: *Changes in Flood Risk in Europe*, edited by: Kundzewicz, Z. W., IAHS Press, Wallingford,
456 121– 166, 2012
- 457 Buzzi, A. and Foschini, L.: Mesoscale meteorological features associated with heavy precipitation in the Southern Alpine
458 Region, *Meteorol. Atmos. Phys.*, 72, 131–146, 2000.
- 459 Chapron E., Simonneau A., Ledoux G., Arnaud F., Lajeunesse P. and Albéric P.: French Alpine Foreland Holocene
460 Paleoseismicity Revealed by Coeval Mass Wasting Deposits in Glacial Lakes. In: G. Lamarche et al. (eds.), *Submarine
461 Mass Movements and their Consequences*, *Advances in Natural and Technological Hazards Research* 41, 341-349,
462 2016.
- 463 Croudace, I. W., Rindby, A., and Rothwell, R. G.: ITRAX: description and evaluation of a new multi-function X-ray core
464 scanner, in: *New Techniques in Sediment Core Analysis*, edited by: Rothwell, R. G., Geological Society, London,
465 *Special Publications*, 367, 51–63, 2006.
- 466 Denniston R.G., Villarini G., Gonzales A.N., Wyrwoll K.H., Polyak V.J., Ummenhofer C.C., Lachniet M.S., Wanamaker Jr.
467 A.D., Humphreys W.F., Woods D. and Cugley J.: Extreme rainfall activity in the Australian tropics reflects changes in
468 the El Niño/Southern Oscillation over the last two millennia. *Proc Natl Acad Sci USA* 112(15):4576–4581, 2015.
- 469 Eva C., Barani S., Carenzo G., De Ferrari R., Eva E., Ferretti G., Pasta M., Pavan M., Scafidi D., Solarino S., Spallarossa D.,
470 Turino C., Zunino E.: 30 years of seismicity in the South-western Alps and Northern Apennines as recorded by the
471 Regional Seismic network of Northwestern Italy. *Proceedings of GNGTS 2010*, Prato, Italy, 2010.
- 472 Fäh, D., Giardini, D., Kästli, P., Deichmann, N., Gisler, M., Schwarz-Zanetti, G., Alvarez-Rubio, S., Sellami, S., Edwards,
473 B., Allmann, B., Bethmann, F., Wössner, J., Gassner-Stamm, G., Fritsche, S., Eberhard, D.: *ECOS-09 Earthquake
474 Catalogue of Switzerland Release 2011. Report and Database*. Public catalogue, 17.4.2011. Swiss Seismological
475 Service ETH Zürich, Report SED/RISK/R/001/20110417, 2011.
- 476 Fanetti, D., F. S. Anselmetti, E. Chapron, M. Sturm, and Vezzoli L.: Megaturbidite deposits in the Holocene basin fill of
477 Lake Como (southern Alps, Italy), *Palaeogeogr. Palaeoclimatol. Palaeoecol.*, 259, 323–340, 2008.
- 478 Gani, M. R.: From turbid to lucid: A straightforward approach to sediment gravity flows and their deposits, *Sediment. Rec.*,
479 2, 4–8, 2004.
- 480 Gaume, E., Bain, V., Bernardara, P., Newinger, O., Barbuc, M., Bateman, A., Blaškovicčová, L., Blöschl, G., Borga, M.,
481 Dumitrescu, A., Daliakopoulos, I., Garcia, J., Irimescu, A., Kohnova, S., Koutroulis, A., Marchi, L., Matreata, S.,
482 Medina, V., Preciso, E., Sempere-Torres, D., Stancalie, G., Szolgay, J., Tsanis, I., Velasco, D. and Viglione, A.: A
483 collation of data on European flash floods. *J. Hydrol.* 367, 70–78, 2009.
- 484 Giguet-Covex C., Arnaud, F., Poulénard, J., Disnar, J.R., Delhon, C., Francus, P., David, F., Enters, 34 D., Rey, P.-J.,
485 Delannoy, J.-J.: Changes of erosion patterns during the Holocene in a currently 35 treeless subalpine catchment inferred
486 from lake sediment geochemistry (Lake Anterne, 2063 m asl, 36 NW French Alps). *The Holocene* 21, 651-665, 2011.



- 487 Gilli, A., Anselmetti, F. S., Glur, L., and Wirth, S. B.: Lake sediments as archives of recurrence rates and intensities of past
488 flood events, in: Dating Torrential Processes on Fans and Cones – Methods and Their Application for Hazard and Risk
489 Assessment, edited by: Schneuwly-Bollschweiler, M., Stoffel, M., and Rudolf-Miklau, F., *Adv. Glob. Change Res.*, 47,
490 225–242, 2012.
- 491 Goldberg, E. D.: *Geochronology with 210Pb Radioactive Dating*, IAEA, Vienna, 121–131, 1963.
- 492 Guidoboni, E., Ferrari, G., Mariotti, D., Comastri, A., Tarabusi, G., and Valensise, G.: Catalogue of strong earthquakes in
493 Italy 461B.C.–1997 and Mediterranean area 760 B.C.–1500, 2007, available from <http://storing.ingv.it/cfti4med>, 2007.
- 494 Guyard H, Chapron E, St-Onge G, Anselmetti, F.S., Arnaud, F., Magand, O., Francus, P. and Melières, MA.: High-altitude
495 varve records of abrupt environmental changes and mining activity over the last 4000 years in the Western French Alps
496 (Lake Bramant, Grandes Rousses Massif). *Quaternary Science Reviews* 26: 2644– 2660, 2007.
- 497 Guzzetti, F. and Tonelli, G.: Information system on hydrological and geomorphological catastrophes in Italy (SICI): a tool for
498 managing landslide and flood hazards. *Natural Hazards and Earth System Sciences* 4, 213–232, 2004.
- 499 Jenny, J.-P., Wilhelm, B., Arnaud, F., Sabatier, P., Giguet-Covex, C., Mélo, A., Fanget, B., Malet, E., Ployon, E., and Perga,
500 M.E., A 4D sedimentological approach to reconstructing the flood frequency and intensity of the Rhône River (Lake
501 Bourget, NW European Alps), *J. Paleolimnol.*, 51, 469–483, 2014.
- 502 Kremer, K., Corella, J.P., Adatte, T., Garnier, E., Zenhäusern, G. and Girardclos S., Origin of turbidites in deep Lake Geneva
503 (France-Switzerland) in the last 1500 years. *J. of Sed. Res.* 85, 1455–1465, 2015.
- 504 Lambert, J., and Levret-Albaret A. : *Mille ans de Séismes en France. Catalogues d’Épicentres, Paramètres et Références*,
505 Ouest-Editions ed., 78 pp., Presses Académiques, Nantes, 1996.
- 506 Lapointe, F., Francus, P., Lamoureaux, S.F., Said, M. and Cuvén, S.: 1,750 years of large rainfall events inferred from
507 particle size at East Lake, Cape Bounty, Melville Island, Canada. *J Paleolimnol* 48(1):159–173, 2012.
- 508 Larroque, C., O. Scotti, and Ioualalen, I.: Reappraisal of the 1887 Ligurian earthquake [western Mediterranean] from
509 macroseismicity, active tectonics and tsunami modelling. *Geophys. J. Int.*, 190, 87–104, 2012.
- 510 Lauterbach, S., Chapron, E., Hüls, M., Gilli, A., Arnaud, F., Piccin, A., Nomade, J., Desmet, M., von Grafenstein, U., and
511 DecLakes Participants: A sediment record of Holocene surface runoff events and earthquake activity from Lake Iseo
512 (Southern Alps, Italy). *Holocene* 22, 749–760, 2012.
- 513 Lionello, P., Abrantes, F., Congedi, L., Dulac, F., Gacic, M., Gomis, D., Goodess, C., Hoff, H., Kutiel, H., Luterbacher, J.,
514 Planton, S., Reale, M., Schröder, K., Struglia, M. V., Toreti, A., Tsimplis, M., Ulbrich, U., and Xoplaki, E.:
515 Introduction: Mediterranean Climate: Background Information, edited by: Lionello, P., *The Climate of the
516 Mediterranean Region, From the Past to the Future*, Amsterdam: Elsevier (Netherlands), XXXV–IXXX,
517 ISBN:9780124160422, 2012.
- 518 Marchi L., Borga M., Preciso E. and Gaume E.: Characterisation of selected extreme flash floods in Europe and implications
519 for flood risk management. *J. of Hydrol.* 394 (1-2), 118-133, 2010..
- 520 Marco, S., Stein, M., Agnon, A., and Ron, H.: Long-term earthquake clustering: A 50,000-year paleoseismic record in the
521 Dead Sea Graben. *Journal of Geophysical Research: Solid Earth*, 101(B3), 6179-6191, 1996.
- 522 Mercalli, L., Cat Berro, D., Montuschi, S., Castellano, C., Ratti, M., Di Napoli, G., Mortara, G., and Guidani, N.: *Atlante
523 climatico della Valle d’Aosta, Societa Meteorologica Subalpina*, Torino, 2003.



- 524 Migowski, C., A. Agnon, R. Bookman, J. F. W. Negendank, and Stein M.: Recurrence pattern of Holocene earthquakes along
525 the Dead Sea transform revealed by varve-counting and radiocarbon dating of lacustrine sediments, *Earth Planet. Sci.*
526 *Let.*, 222(1), 301–314, 2004.
- 527 Moernaut, J., M. Van Daele, K. Heirman, K. Fontijn, M. Strasser, M. Pino, R. Urrutia, and De Batist M.: Lacustrine
528 turbidites as a tool for quantitative earthquake reconstruction: New evidence for a variable rupture mode in south
529 central Chile, *J. Geophys. Res. Solid Earth*, 119, 1607–1633, 2014.
- 530 Monecke, K., F. S. Anselmetti, A. Becker, M. Sturm, and Giardini D.: The record of historic earthquakes in lake sediments of
531 Central Switzerland, *Tectonophysics*, 394, 21–40, 2004.
- 532 Morgenstern, N. R.: *Submarine Slumping and Initiation of Turbidity Currents*, edited by A. F. Richards, pp. 189–220, Mar.
533 Geotechnique UP, Urbana, Ill, 1967.
- 534 Mulder, T., and E. Chapron: Flood deposits in continental and marine environments: Character and significance, in *Sediment*
535 *Transfer From Shelf to Deep Water—Revisiting the Delivery System RM*, AAPG Stud. Geol., vol. 61, edited by S. C.
536 Zavala, 1–30, 2011.
- 537 Mulder, T., and P. Cochonat: Classification of offshore mass movements, *J. Sediment. Res.*, 66(1), 43–57, 1996.
- 538 Munich Re Group: Annual review: natural catastrophes 2002. Munich Re Group, Munich, p 62, 2003.
- 539 Passega, R.: Grain-size representation by CM patterns as a geological tool, *J. Sediment. Petrol.*, 34, 830–847, 1964.
- 540 Petersen, J., B. Wilhelm, M. Revel, Y. Rolland, C. Crouzet, F. Arnaud, E. Brisset, E. Chaumillon, and Magand O.: Sediments
541 of Lake Vens (SW European Alps, France) record large-magnitude earthquake events, *J. Paleolimnol.*, 51(3), 343–355,
542 2014.
- 543 Renberg, I., R. Bindler, and Bränvall M.L.: Using the historical atmospheric lead-deposition record as a chronological marker
544 in sediment deposits in Europe, Holocene, 11(5), 511–516, 2001.
- 545 Ratto, S., Bonetto, F., and Comoglio, C.: The October 2000 flooding in Valle d'Aosta (Italy): Event description and land
546 planning measures for the risk mitigation. *International Journal of River Basin Management*, 1(2), 105–116, 2003.
- 547 Rizza, M., Ritz, J. F., Braucher, R., Vassallo, R., Prentice, C., Mahan, S. and Demberel, S.: Slip rate and slip magnitudes of
548 past earthquakes along the Bogd left-lateral strike-slip fault (Mongolia). *Geophysical Journal International*, 186(3),
549 897–927, 2011.
- 550 Rodriguez-Pascua, M. A., V. H. Garduno-Monroy, I. Israde-Alcantara, and Pérez-Lopez R.: Estimation of the paleoepicentral
551 area from the spatial gradient of deformation in lacustrine seismites (Tierras Blancas Basin, Mexico), *Quat. Int.*, 219,
552 66–78, 2010.
- 553 Schiefer, E., Gilbert, R., and Hassan, M. A.: A lake sediment-based proxy of floods in the Rocky Mountain Front Ranges,
554 Canada, *J. Paleolimnol.*, 45, 137–149, 2011.
- 555 Schillereff, D. N., Chiverrell, R. C., Macdonald, N., and Hooke, J. M.: Flood stratigraphies in lake sediments: A
556 review. *Earth-Science Reviews*, 135, 17–37, 2014.
- 557 Schillereff, D. N., Chiverrell, R. C., Macdonald, N., and Hooke, J. M.: Hydrological thresholds and basin control over
558 paleoflood records in lakes. *Geology*, 44(1), 43–46, 2016.
- 559 Schmidt, S., H. Howa, A. Diallo, J. Martín, M. Cremer, P. Duros, Ch. Fontanier, B. Deflandre, E. Metzger, and Mulder T.:
560 Recent sediment transport and deposition in the Cap-Ferret Canyon, South-East margin of Bay of Biscay, *Deep Sea*
561 *Research II*, 104, 134–144, doi:10.1016/j.dsr2.2013.06.004, 2014.



- 562 Schnellmann, M., F. S. Anselmetti, D. Giardini, and McKenzie J. A.: Mass-movement-induced fold-and-thrust belt structures
563 in unconsolidated sediments in Lake Lucerne (Switzerland), *Sedimentology*, 52, 271–289, 2005.
- 564 Scotti, O., D. Baumont, G. Quenet, and Levret A.: The French macroseismic database SISFRANCE: Objectives, results and
565 perspectives, *Ann. Geophys.*, 47(2), 571–581, 2004.
- 566 Shiki, T., Kumon, F., Inouchi, Y., Kontani, Y., Sakamoto, T., Tateishi, M. and Fukuyama, K.: Sedimentary features of the
567 seismo-turbidites, Lake Biwa, Japan. *Sedimentary Geology*, 135(1), 37–50, 2000.
- 568 Simonneau, A., Chapron, E., Vannière, B., Wirth, S. B., Gilli, A., Di Giovanni, C., Anselmetti, F. S., Desmet, M., and
569 Magny, M.: Mass-movement and flood-induced deposits in Lake Ledro, southern Alps, Italy: implications for
570 Holocene palaeohydrology and natural hazards, *Clim. Past*, 9, 825–840, 2013.
- 571 Støren, E. N., Olaf Dahl, S., Nesje, A., and Paasche Ø.: Identifying the sedimentary imprint of high-frequency Holocene river
572 floods in lake sediments: development and application of a new method, *Quaternary Sci. Rev.*, 29, 3021–3033, 2010.
- 573 Strasser, M., F. S. Anselmetti, F. Donat, D. Giardini, and Schnellmann M.: Magnitudes and source areas of large prehistoric
574 northern Alpine earthquakes revealed by slope failures in lakes, *Geology*, 12, 1005–1008, 2006.
- 575 Strasser, M., M. Hilbe, and Anselmetti F.S.: Mapping basin-wide subaquatic slope failure susceptibility as a tool to assess
576 regional seismic and tsunami hazards, *Mar. Geophys. Res.*, 32, 331–347, 2011.
- 577 Strasser, M., K. Monecke, M. Schnellmann, and Anselmetti F.S.: Lake sediments as natural seismographs: A compiled
578 record of Late Quaternary earthquakes in Central Switzerland and its implication for Alpine deformation,
579 *Sedimentology*, 60, 319–341, 2013.
- 580 Sturm, M., and Matter A.: Turbidites and varves in Lake Brienz (Switzerland): Deposition of clastic detritus by density
581 currents, in *Modern and Ancient Lake Sediments*, edited by A. Matter and M. E. Tucker, Int. Assoc. Sedimentol. Spec.
582 Publ., 2, 147–168, 1978.
- 583 Ratzov, G., Cattaneo, A., Babonneau, N., Déverchère, J., Yelles, K., Bracene, R., & Courboux, F.: Holocene turbidites
584 record earthquake supercycles at a slow-rate plate boundary. *Geology*, 43(4), 331–334, 2015.
- 585 Van Daele, M., Moernaut, J., Doom, L., Boes, E., Fontijn, K., Heirman, K., Vandoorne, W., Hebbeln, D., Pino, M., Urrutia,
586 R., Brümmer, R., and De Batist, M.: A comparison of the sedimentary records of the 1960 and 2010 great Chilean
587 earthquakes in 17 lakes: Implications for quantitative lacustrine palaeoseismology, *Sedimentology*, 62, 1466–1496,
588 2015.
- 589 Vanniere, B., Magny, M., Joannin, S., Simonneau, A., Wirth, S. B., Hamann, Y. and Anselmetti, F. S.: Orbital changes,
590 variation in solar activity and increased anthropogenic activities: controls on the Holocene flood frequency in the Lake
591 Ledro area, Northern Italy. *Climate of the Past*, 9(3), 1193–1209, 2013.
- 592 Weiss, D., Shotyk, W., Kramers, J. D., and Gloor, M.: Sphagnum mosses as archives of recent and past atmospheric lead
593 deposition in Switzerland. *Atmospheric Environment*, 33(23), 3751–3763, 1999.
- 594 Wiemer, G., J. Moernaut, N. Stark, P. Kempf, M. De Batpist, M. Pino, R. Urrutia, B. Ladrón de Guevara, M. Strasser, and
595 Kopf A.: The role of sediment composition and behavior under dynamic loading conditions on slope failure initiation:
596 A study of a subaqueous landslide in earthquake-prone South-Central Chile, *Int. J. Earth Sci.*, 104(5), 1439–1457,
597 2015.
- 598 Wilhelm, B., Arnaud, F., Sabatier, P., Crouzet, C., Brisset, E., Chaumillon, E., Disnar, J. R., Guiter, F., Malet, E., Reys, J. L.,
599 Tachikawa, K., Bard, E., and Delannoy, J. J.: 1400 years of extreme precipitation patterns over the Mediterranean
600 French Alps and possible forcing mechanisms, *Quaternary Res.*, 78, 1–12, 2012a.



- 601 Wilhelm, B., F. Arnaud, D. Enters, F. Allignol, A. Legaz, O. Magand, S. Revillon, C. Giguet-Covex, and Malet E.: Does
602 global warming favour the occurrence of extreme floods in European Alps? First evidences from a NW Alps proglacial
603 lake sediment record, *Clim. Change*, 113, 63–581, 2012b.
- 604 Wilhelm, B., Arnaud, F., Sabatier, P., Magand, O., Chapron, E., Courp, T., Tachikawa, K., Fanget, B., Malet, E., Pignol, C.,
605 Bard, E., and Delannoy, J. J.: Palaeoflood activity and climate change over the last 1400 years recorded by lake
606 sediments in the NW European Alps, *J. Quat. Sci.*, 28, 189–199, 2013.
- 607 Wilhelm, B., P. Sabatier, and Arnaud F.: Is a regional flood signal reproducible from lake sediments?, *Sedimentology*, 62(4),
608 1103–1117, 2015.
- 609 Wilhelm B., Vogel H., Crouzet C., Etienne D. and Anselmetti F.S.: Frequency and intensity of palaeofloods at the interface
610 of Atlantic and Mediterranean climate domains, *Climate of the Past* 12, 299-316, 2016a.
- 611 Wilhelm, B., Nomade, J., Crouzet, C., Litty, C., Sabatier, P., Belle, S. and Anselmetti, F.S.: Quantified sensitivity of small
612 lake sediments to record historic earthquakes: Implications for paleoseismology. *J. Geophys. Res.: Earth Surface*, 121
613 (1), 2-16, 2016b.
- 614 Wirth, S. B., Gilli, A., Simonneau, A., Ariztegui, D., Vannière, B., Glur, L., Chapron, E., Magny, M., and Anselmetti, F. S.:
615 A 2000-year long seasonal record of floods in the southern European Alps, *Geophys. Res. Lett.*, 40, 4025–4029, 2013.